Tabriz Journal of Electrical Engineering (TJEE), vol. 55, no. 4, 2025 Serial no. 114
DOI: 10.22034/tjee.2025.64094.4908

Integral Backstepping Sliding Mode Control of Influenza Epidemic in the Presence of Input Saturation and External Disturbances

F. Nobakht, H. Eliasi*

Department of Electrical and Computer Engineering, University of Birjand, Birjand, Iran.
E-mail: Fariba.nobakht@birjand.ac.ir, H_eliasi@birjand.ac.ir
*Corresponding author

Received: 20/10/2024, Revised: 19/01/2025, Accepted: 05/03/2025

Abstract
This paper presents a robust sliding mode control approach based on integral backstepping for multi-input multi-output (MIMO) nonlinear systems. The proposed control scheme addresses input saturation, modeling uncertainties, and time-varying external disturbances. A novel auxiliary design system and Nussbaum gain functions are incorporated into the control scheme to tackle input saturation. The proposed control approach is applied to a nonlinear epidemic model. The model of Flu epidemiology, which includes five non-negative state variables representing the susceptible, exposed, infected, asymptomatic, and recovered individuals, along with three control inputs for vaccination, medical treatment, and social distancing, is being studied. Simulation results demonstrate the effectiveness of the proposed control scheme in handling input saturation and achieving accurate trajectory tracking, highlighting its potential for uncertain nonlinear systems with input constraints.

Keywords
Backstepping sliding mode control, Input saturation, Nussbaum function, Influenza epidemic.

Introduction

Mathematical modeling has proven to be a powerful tool in studying the dynamics of infectious diseases. By constructing simplified representations of disease transmission, epidemic models enable researchers to gain insights into the spread and behavior of diseases. These models facilitate predictions of epidemics, including estimates of infections, hospitalizations, and fatalities. Moreover, they aid in evaluating the efficacy of various control strategies, contributing to informed decision-making during outbreaks [1]. However, selecting the most appropriate model can be challenging, as researchers utilize deterministic and stochastic models to gain insights into unexpected behaviors and epidemic progression [2, 3, 4]. The choice of model depends on the specific research question, data availability, and desired level of complexity.

Different control strategies have been implemented to address epidemics, such as social distancing, lockdowns, cleanliness, handwashing, face masks and shields, lab tests, contact tracing, and monitoring infected and exposed individuals. Different types of controllers have been created for infectious disease models.

Optimal control theory is a mathematical optimization technique that can be used to determine the best way to control the spread of an epidemic. It involves finding the combination of control measures that will minimize the total cost of the epidemic, which includes the cost of implementing the control measures themselves as well as the cost of the damage caused by the epidemic [5]. For instance, an optimal control of the SEIQR epidemic model with two groups of individuals, which includes a nonlinear saturated incidence rate and considers two control measures of vaccination and treatment of infected individuals, is developed in [6]

An optimal control framework for influenza epidemics, including preventive measures and antiviral treatment is developed in [7]. It emphasizes the effectiveness of these controls in reducing infection rates and associated costs, suggesting that further discussion on recent control schemes could enhance understanding of their implementation. The results showed that optimal control strategies can significantly reduce the disease burden and mitigate the impact of influenza epidemics.

The other approaches for epidemic suppression include impulsive control [2] , predictive control, fuzzy control [8], phase-lead/phase-lag control [9], as well as input-output linearization [10]. Predictive control can provide accurate predictions of the spread of infectious diseases, allowing public health officials to make informed decisions about interventions. An infectious disease dynamic prediction model with control variables (SEIR-CV), which considers the characteristics of the influenza epidemic transmission, seasonal impacts, and the intensity changes of control measures over time is presented in [11].

The control strategies mentioned earlier were developed, assuming all dynamic terms and parameters are fully known. However, the parameters of the pandemic model are uncertain due to factors such as disease spread rates, mortality rates, and contact rates among individuals. These factors are not fixed and can change based on social and disease-related factors [12]. Thus, these unknown variables must be considered when implementing

measures to control a disease outbreak. To overcome these challenges, robust and adaptive control techniques are used to achieve stable performance even when there are uncertainties in the model. For example, in [13], a nonlinear robust adaptive sliding mode control of influenza epidemic is developed, considering two control measures: vaccination and treatment of infected individuals. The proposed control strategy combines the advantages of sliding mode control and adaptive control to achieve robust control performance in the presence of uncertainties and disturbances. A robust optimal control strategy for influenza epidemics using an extended maximum correntropy Kalman filter for state estimation, combined with a quadratic program optimization to minimize susceptible and infected individuals while managing vaccination and treatment rates is developed in [14].

In recent studies on adaptive and robust control, the backstepping design offers a structured approach for developing tracking and regulation strategies [15, 16, 17]. Backstepping is a method based on Lyapunov recursion for systems classified as 'strict-feedback.' Backstepping is a control design technique that employs a recursive approach. In this method, specific state variables are considered virtual controls, and intermediate control laws are formulated for these virtual controls. By iteratively applying this procedure, the overall control law is constructed systematically. This method can achieve and enhance transient performance by deliberately adjusting design parameters [18]. Unfortunately, the backstepping control system cannot achieve robustness against model uncertainties and external disturbances.

Sliding mode control (SMC) is a powerful technique for controlling nonlinear systems due to its robustness to parameter variations and disturbances [1, 3, 19]. However, the conventional SMC approach using the Sign function as the switching function can lead to chattering, which is undesirable and can affect system stability. Mitigating chattering is a critical challenge in the design of SMC systems, and various techniques have been developed to address this issue, such as boundary layer methods, hysteresis-based approaches, using other switching functions, such as saturation, and higher-order sliding mode control [20].

The backstepping method combined with sliding mode control (BSMC) can efficiently address issues arising from parameter uncertainties in the epidemic disease model and enhance the stability of the control system [21, 22, 23]. Backstepping sliding mode control divides the nonlinear system into multiple subsystems. Sliding mode control is implemented for every subsystem using the Lyapunov function to ensure the convergence of position-tracking errors under any initial condition. The integrator backstepping technique offers several advantages in control system design. Transforming a nonlinear system into a strict feedback form simplifies the control problem and allows for the systematic design of stabilizing controllers [20, 24]. Combining integrator backstepping with sliding mode control further enhances system performance by eliminating chattering in the control input and improving robustness against modelling uncertainties and external disturbances. Adding an integrator in the control structure enhances the system's ability to achieve accurate steady-state control, making it a valuable technique in various control applications.

Input saturation is a common phenomenon in real-world control systems, where the control inputs are subject to physical constraints. In the context of the proposed control approach for influenza epidemics, input saturation can arise due to limitations in the availability of resources for vaccination, antiviral therapy, and social distancing measures. For instance, there may be constraints on the production and distribution of vaccines, the capacity of healthcare facilities to administer antiviral treatments, or the willingness of individuals to comply with social distancing guidelines. These limitations can affect the effectiveness of control measures and introduce nonlinearities into the model, making it challenging to accurately predict the epidemic's course. Therefore, it is essential to consider actuator saturation when developing and analyzing epidemiological models to ensure accurate predictions and effective decision-making.

To mitigate the adverse consequence of input constraints in epidemiological models, anti-windup compensator (AWC) techniques are employed. These techniques maintain system stability and performance despite input constraints [20]. By incorporating anti-windup mechanisms, the controller can adapt to saturation conditions and regulate the system's behavior effectively, ensuring accurate predictions and adequate decision-making in the face of actuator limitations. Anti-windup controller techniques can be broadly classified into one-step approaches and two-step design procedures. One-step approaches create feedback controllers that account for saturation; simultaneously, two-step design procedures involve designing an optimal controller without considering saturation and augmenting it with anti-windup compensation. Anti-windup controllers in epidemic models provide several advantages in preventing windup, improving stability, enhancing robustness, achieving better tracking performance, and applying it to nonlinear systems. These advantages make anti-windup controllers valuable for controlling and managing epidemic models [17].

Various approaches have been proposed for anti-windup controller design. Guo et al. [25] proposed an adaptive second-order backstepping control algorithm for a two-degrees-of-freedom underactuated system. An adaptive backstepping sliding mode tracking control method for underactuated unmanned surface vehicles is suggested in [26]. Neisarian et al. [27] proposed a new rapid finite-time velocity observer-based terminal sliding mode controller for a group of MIMO nonlinear systems with unknown time-varying bounded matched uncertainties and input saturation constraints. Wan et al. [20] introduced integral backstepping sliding mode control for unmanned autonomous helicopters when dealing with input saturation. These approaches aim to ensure that the control system with saturating actuators closely follows the output of the unsaturated system.

This research article proposes a novel nonlinear anti-windup control method that utilizes integral backstepping combined with the sliding mode control to stabilize the

nonlinear MIMO epidemic system under input saturation and external disturbances. The anti-windup compensator is designed based on a one-step strategy. The backstepping control algorithm presented by Wen et al. [18] is adopted and modified to develop the integral backstepping sliding mode controller (IBSMC) for MIMO epidemic systems. By considering the complexities of real-world scenarios, where control inputs may be subject to constraints or limitations, this study aims to enhance the accuracy and reliability of epidemiological models. The IBSMC combines the strengths of backstepping, sliding mode control, and integral action to achieve robust control that can effectively reject uncertainties and external disturbances. Moreover, the suggested method follows a systematic design procedure, simplifying implementation and analysis compared to other ad-hoc methods. This approach involves decomposing the system into a cascade of subsystems and introducing integral action to eliminate steady-state errors. Sliding mode control provides robustness against uncertainties and external disturbances by forcing the system states to converge to a predefined sliding surface where the system dynamics are insensitive to uncertainties. The specific parameter uncertainties IBSMC addresses in epidemic models include uncertainties in the transmission rate, recovery rate, and initial conditions. These uncertainties can arise from various factors, such as variations in individual behavior, environmental conditions, and the accuracy of data collection. By incorporating these uncertainties, the model provides a more realistic representation of the disease spread and allows for the development of robust control strategies to handle unexpected changes in the disease dynamics. IBSMC can effectively handle these uncertainties and ensure the robustness of the control system.

An additional system was utilized in this paper to manage input saturation and prevent actuator failures. Please note that saturation is not a smooth function, yet the backstepping technique necessitates that all functions be differentiable. To utilize the method, a continuous function is employed to estimate the saturation with a limited approximation error, and subsequently, the system is expanded to develop controllers. Nevertheless, dealing with the derivative of the estimated function poses a problematic challenge regarding design and stability analysis. A Nussbaum function is employed to address the issue. The suggested IBSMC control scheme allows the system to precisely follow a specified path while also gaining robustness against external disruptions and uncertainties that could impact the system manner.

The research presents a deterministic model including five groups of individuals and three control methods: vaccination, antiviral treatment, and social distancing. The model accounts for birth and mortality, allowing the host population to vary over time. The controller aims to bring the number of susceptible, infected, and exposed individuals down to zero by following specific scenarios even when input saturation occurs. This decrease also results in a reduction in the number of asymptomatic individuals, which approaches zero. At the same time, the population that has been restored reaches its peak stable level while following the overall population trend. Some contributions and advantages of this paper are as follows:

- A robust backstepping sliding mode controller was developed for controlling MIMO epidemic systems influenced by input saturation, time-varying external disturbances, and uncertainties.
- By considering uncertainties in the model's nonlinear dynamics, the controller can better handle variations and unexpected changes in the disease transmission process, leading to improved control performance and resilience in real-world challenges.
- To address actuator saturation, the proposed control approach incorporates a novel auxiliary design system and Nussbaum gain functions. These techniques enable the control system to handle input saturation effectively, ensuring that the desired control objectives are achieved despite the presence of input constraints.
- The model considers a time-varying total population ($\dot{N}(t) \neq 0$). Moreover, the birth and natural death rates and the recovered individual's lost immunity after a finite period are critical factors considered in our mathematical models of infectious disease transmission. These factors can significantly impact the dynamics of the disease and the effectiveness of control measures.

The remainder of this paper is split into five parts. In Section 2, we introduce and explain the dynamic SEIAR model in detail, and the result related to the positivity property of such a model is proven. The positivity property is required from the nature of the system, which forbids the existence of hostile populations at any time. The design of integral backstepping sliding mode control for the MIMO nonlinear system is investigated in section 3. Section 4 presents numerical simulation results demonstrating the applicability of the proposed anti-windup control approach to the nonlinear. Finally, we conclude our work in Section 5.

SEIAR Epidemic Model and Problem Statement

This section presents a novel SEIAR epidemic model considering birth and natural death rates.

2.1. Nonlinear SEIAR Model with Dynamic Population

The suggested epidemic model is built on a SEIAR model, expanding the typical SEIR model outlined in [10]. The SEIAR model involves the added aspect that those in the exposed stage who are infected can either show symptoms and move to a contagious stage or show no symptoms and move to an asymptomatic infectious stage. The nonlinear system that describes the dynamics of influenza is represented by:

$$\begin{aligned}
\dot{S}(t) &= -\frac{\beta SI}{N} - \mu S + \upsilon N + \omega R(t), \\
\dot{E}(t) &= \frac{\beta SI}{N} - (\kappa + \mu)E, \\
\dot{I}(t) &= p\kappa E - (\gamma + \mu)I, \\
\dot{A}(t) &= (1-p)\kappa E - (\eta + \mu)A, \\
\dot{R}(t) &= \gamma(1-\rho)I + \eta A - (\mu + \omega)R,
\end{aligned} \tag{1}$$

As a result, this system includes five state variables that have positive values and start with initial conditions: $S(0) = S_0, E(0) = E_0, I(0) = I_0, A(0) = A_0, R(0) = R_0$.

The Susceptible, Exposed, Infected (symptomatic), Asymptomatic, and Recovered compartments are denoted by the positive state variables $S(t), E(t), I(t), A(t),$ and R(t) respectively.

These state variables represent the different compartments in the SEIAR epidemiological model, which describes the dynamics of an influenza outbreak within a population. S denotes the number of individuals that are susceptible (i.e. they are not infected yet), E represents the number of people exposed to infection (they are infected but they cannot transmit the virus), I, represents the number of infected individuals with symptoms, A exhibits the number of asymptomatic carriers, R represents the number of individuals who have recovered from the infection and are assumed to be immune. *N* represents the total population at time t. (i.e., $N(t) = S(t) + E(t) + I(t) + A(t) + R(t)$).

The model equations describe how susceptible individuals (S) come into contact with infected individuals (I) at a rate of β, causing them to transition to the exposed group (E). People who are exposed get infected at a rate of κ and are divided into two groups: those who are infected and those who are carriers without symptoms. A portion of the individuals who have been exposed enters the infected area, while the rest enters the asymptomatic area as described in [1].

People who do not show symptoms (A) transition from their group to the recovered category (R) at a rate of η. Infected individuals (I) also depart from their group at a rate of γ, with a proportion of $(1-\rho)$ recovering and the remaining proportion (ρ) succumbing to the infection. The model takes into account the decreasing immunity of people who have recovered, using parameter ω to determine how long immunity lasts on average. Following this timeframe, individuals who have recovered move back to the group of susceptible individuals. The symbol υ represents the birth rate, and individuals in all groups undergo natural mortality at a rate of μ. Table I specifies that all variables in the model are constant and positive, such as β, κ, p, γ , η and ω. These parameters can be arranged into a single vector θ as follows:

$\theta = [\mu\ \omega\ \upsilon\ \gamma\ \kappa\ \rho\ p\ \eta\ \beta]^T$

in such a way that the SEIAR model (1) can be written as

$$\dot{x}(t) = F(x(t), \theta), x = [\,S\ E\ I\ A\ R]^T \quad (2)$$

Highlighting its explicit dependence on the parameters, θ. It is essential to recognize that the specific values of the parameters in θ are not known, so a nominal set of parameters $\hat{\theta}$ is employed to determine control inputs instead of the real ones. the transmission dynamics of the SEIAR epidemiological model are presented in Fig.1.

The total population dynamics at time t can be calculated by summing up all the equations (1), which leads to

$$\dot{N}(t) = (\nu - \mu)N(t) - \rho\gamma I(t) \quad (3)$$

So that the total population is time-varying.

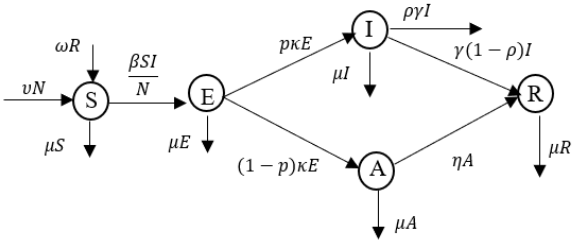

Fig. 1. Conceptual flow diagram of the SEIAR model with death/birth rate.

We expand the SEIAR model by incorporating parallel interventions such as vaccination and antiviral treatment and social distancing strategies such as closing schools, imposing travel restrictions, and cancelling significant public events, defined by the following system of differential equations.

$$\begin{aligned}
\dot{S}(t) &= -\frac{\beta SI\big(1 - sat(u_2(t))\big)}{N} - \mu S + \upsilon N + \omega R(t) \\
&\quad -Nsat(u_1(t)) + \Delta d_1(t) \\
\dot{E}(t) &= \frac{\beta SI(1 - sat(u_2(t))}{N} - (\kappa + \mu)E + \Delta d_2(t) \\
\dot{I}(t) &= p\kappa E - (\gamma + \mu)I - sat(u_3(t))I + \Delta d_3(t) \\
\dot{A}(t) &= (1-p)\kappa E - (\eta + \mu)A + \Delta d_4(t) \\
\dot{R}(t) &= \gamma(1-\rho)I + \eta A - (\mu + w)R + Nsat(u_1(t)) \\
&\quad +sat(u_3(t))I + \Delta d_5(t)
\end{aligned} \quad (4)$$

The equations include three control inputs, $0 \le u_1(t) \le 1, 0 \le u_2(t) \le 1$, and $0 \le u_3(t) \le 1$, crucial in achieving the desired outcome. The control function $u_1(t)$ quantifies the rate at which the total population is vaccinated. Similarly, the control function $u_2(t)$ effectively reduces the contact rate due to social distancing measures. The control function $u_3(t)$ measures the rate at which infectious individuals receive treatment in each period, aiding recovery. The saturation function of the control inputs ($i.e., sat(u_j), j = 1, \cdots, 3$) is defined as follows:

$$sat(u_i(t)) = \begin{cases} sign(u_i(t))u_{M_i}, & |u_i(t)| \ge u_{M_i} \\ u_i(t), & |u_i(t)| < u_{M_i} \end{cases} \quad (5)$$

Where u_{M_i} are the known bounds of the ith input, u_i, The vector of perturbation caused by uncertainties, unmodeled dynamics, and time-varying external disturbances, denoted as $\Delta d(t)$, plays a crucial role in enhancing the robustness and accuracy of the model. By considering various sources of uncertainties and disturbances, such as travel and migration, changes in public health policies, variations in model parameters, and economic factors, the model can better capture the complexities and dynamics of the real world. This leads to more reliable predictions and improved decision-making capabilities. It is assumed that the maximum value of $\Delta d(t)$ is known and bounded by d_{max} ($|\Delta d| \le d_{max}$). Our proposed control strategy aims to track desired descending reference signals for the state variables $S, E,$ and I. Therefore, the controller seeks to reduce the number of susceptible, exposed, and infected individuals to zero ($S \to 0, E \to 0, and\ I \to 0$) by monitoring specific situations and utilizing vaccination, antiviral treatment, and social distancing as inputs. In these circumstances, it is demonstrated that the state variables are limited and approach zero ($A \to 0$). Due to the decline in the mentioned influenza sections

$(S, E, I,$ and $A)$, the removed-by-immunity population asymptotically tracks the whole population $(R \to N)$.

2.2. Positivity and Boundedness of the Solution

For an epidemic model to be effective for potential uses, it must have positive solutions and be bounded. Therefore, system (1) solutions need to be constrained to being positive and bounded based on the provided initial conditions:

$(S(0), E(0), I(0), A(0), R(0)) \in R_5^+$

Proposition 1. In the orthant of R_5^+, the system (1) has to be positive and invariant.

Proof. When the value of S reaches zero at a time, 't,' all other state variables are reset to zero. At time t, S signifies this.

$\dot{S}(t)\big|_{S(t)=0} = \upsilon N + \omega R \geq 0$

Due to the positivity of the model parameters, the number of recovered individuals, and the total population, S will only increase and not decrease. In the same way, the remaining state variables are also visible.

$\dot{E}(t)\big|_{E(t)=0} = \frac{\beta SI}{N} \geq 0$

$\dot{I}(t)\big|_{I(t)=0} = p\kappa E \geq 0$

$\dot{A}(t)\big|_{A(t)=0} = (1-p)\kappa E \geq 0$

$\dot{R}(t)\big|_{R(t)=0} = \gamma(1-\rho)I + \eta A \geq 0$

As a result, in R_5^+, all of the state variables are non-negative and invariant set for the model (1).

Proposition 2. In the feasible region Γ, the system (1) is bounded.

$$\Gamma = \left\{ (S, E, I, A, R) \epsilon R_5^+ : 0 \leq S + E + I + A + R \leq \frac{\Lambda}{\mu} \right\}$$

Proof. The sum of all equations in the model (1) results in the following equation for the total population.

$\dot{N}(t) = (\nu - \mu)N(t) - \rho\gamma I(t)$

$N(t) \leq N(0)e^{-\mu t} + \frac{\Lambda}{\mu}(1 - e^{-\mu t})$

$N(t) \leq \frac{\Lambda}{\mu}, \quad if\ N(0) \leq \frac{\Lambda}{\mu}$

Where $\Lambda = \nu N(t) - \rho\gamma I(t)$. It can be verified that Γ is positively invariant with respect to (1).

2.3. Basic Reproduction Number

In epidemic theory, the basic reproduction number, commonly denoted as R_0, is one of the most critical concepts due to its ability to predict the course of an epidemic. It represents the average number of secondary infections caused by a single infected individual during their infectious period. The value of R_0 is instrumental in determining the stability of operating points. If $R_0 < 1$, the disease-free equilibrium is locally asymptotically stable, indicating that the epidemic will self-eradicate. If $R_0 > 1$, the disease-free equilibrium is unstable, and there will always be a non-zero number of infectious individuals within the population. System (1) always has the disease-free equilibrium. To find this equilibrium, all infected variables must be set to zero $(i.e., E = I = A = 0)$ and the remaining variables are solved accordingly. Thus, the equilibrium of the population in the absence of disease is obtained as follows:

$Q_0 = (\frac{\nu N}{\mu}, 0, 0, 0, 0)$

One common approach to calculating R_0 is the next-generation matrix method. This method involves constructing a matrix that represents the average number of new infections generated by an infected individual across each compartment of the epidemiological model. Let $\chi(t) = [E\ I\ A]^T$,Then, the dynamics of the system can be described by the following equations:

$$\dot{\chi}_i = \mathcal{F}_i(\chi) - \mathcal{V}_i(\chi) \quad (6)$$

Here, $\mathcal{F}_i(\chi)$ represents the rate of appearance of new individuals in group i ,while $\mathcal{V}_i(\chi)$ signifies the difference between the rate at which individuals enter group (i) and the rate at which they leave it. The non-negative matrices F and V as $F = \left[\frac{\partial \mathcal{F}_i}{\partial x_j}\right]$ and $V = \left[\frac{\partial \mathcal{V}_i}{\partial x_j}\right]$ are calculated as follows:

$$F = \begin{bmatrix} 0 & \frac{\beta S}{N} & 0 \\ 0 & 0 & 0 \\ 0 & 0 & 0 \end{bmatrix}, V = \begin{bmatrix} (\kappa + \mu) & 0 & 0 \\ -p\kappa & (\gamma + \mu) & 0 \\ -(1-p)\kappa & 0 & (\eta + \mu) \end{bmatrix}$$

Set $R_0 = \rho(FV^{-1})$, where $\rho(\mathrm{A})$ denotes the spectral radius of matrix A. Thus, the basic reproduction ratio for individuals suffering from serious disease is given by:

$$R_0 = \frac{\beta p \kappa \nu}{\mu(\mu+\gamma)(\mu+\kappa)} \quad (7)$$

Design of robust controller

3.1. System Description and Preliminaries

Consider the following class of MIMO continuous-time nonlinear plant as follows:

$$\dot{x}(t) = f\big(x(t)\big) + \sum_{i=1}^{m} g_i(x(t)) sat(u_i(t)) + \Delta d\big(x(t)\big),$$

$$y_j(t) = h_j\big(x(t)\big),$$

$$i = j = 1, 2, \cdots, m \quad (8)$$

Where $y(t) \in \mathbb{R}^m, u(t) \in \mathbb{R}^m$, and $x(t) \in \mathbb{R}^n$ are the output signal vector, the input signal vector, and the system's state vector, respectively. $f(x(t))$ is a smooth vector field, $g(x(t))$ is a smooth $m \times m$ nonlinear matrix. The control objective is to design a robust control scheme such that the outputs $y_j(t)$ track the desired trajectory $y_{d_j}(t)$. Tracking errors should always remain within given constraints while ensuring the boundedness of all closed-loop signals.

1.2. Backstepping Control

Backstepping is a recursive design mechanism that enables the asymptotic stabilization of a controller for systems in strict feedback form. The fundamental concept behind backstepping design involves decomposing a complex nonlinear system into smaller subsystems, ensuring that the degree of each subsystem does not surpass that of the entire system. This decomposition facilitates the design of a Lyapunov function and virtual control for each subsystem, ultimately leading to the construction of the overall control system through backstepping. To design an appropriate backstepping controller, it is essential to derive the strict feedback form of the control system [21]. In cases where the nonlinear system is not in a strict feedback form, input-output linearization or alternative methods can be employed to transform the system into the desired standard form [23].This transformation enables the application of backstepping design techniques, facilitating the

development of an effective controller for the nonlinear system. Assume that the system (8) is transformed into the following parametric-strict-feedback system with zero dynamics via a diffeomorphism $[\psi^T, \eta^T]^T = \Phi(x)$ as follows

$$\dot{\eta} = q(\eta, \psi) \tag{9}$$

$$\dot{\psi}_k^j = \psi_{k+1}^j, \quad 1 \le k \le r_j - 1, \ 1 \le j \le m$$

$$\dot{\psi}_{r_j}^j = b_j(\eta, \psi) + \sum_{i=1}^{m} a_{ji}(\eta, \psi) sat(u_i) + \Delta d_j(t),$$

$$1 \le j \le \mathrm{m} \tag{10}$$

Where $\eta(t) = [\eta_{r+1}(t) \ \eta_{r+2}(t) \ \cdots \ \eta_n(t)]^T$ and $q(\eta, \psi)$, $b_j(\eta, \psi) = L_f^{r_j} h_j(x)$ are smooth vector functions, $a_{ji}(\eta, \psi) = L_{g_i} L_f^{r_j - 1} h_j(x)$ is $j, i - th$ array of a known non-singular $m \times m$ matrix which represented by $\mathrm{A}(\eta, \psi)$ for all $[\psi^T, \eta^T]^T \in \mathbb{R}^n$. The integer r_j denotes the smallest relative degree of the jth output concerning any of the m inputs, $r = r_1 + r_2 + \cdots + r_m$ is defined as the sum of individual relative degrees.

The control goal is to design a state feedback robust controller for the uncertain nonlinear system in the presence of input saturation and disturbance such that the output y_i tracks a desired trajectory y_{d_j}; in contrast, all signals in the closed-loop systems are bounded. The relationship between the applied control $sat(u_i(t))$, and the control input $u_i(t)$ exhibits a sharp discontinuity when its absolute value of $u_i(t)$ reaches the saturation level u_{M_i}. This discontinuity poses a challenge for directly applying the backstepping technique. To overcome this issue, we approximate the saturation function with a smooth function. One commonly used approximation is the hyperbolic tangent function, defined as [18].

$$g(u_i) = u_{M_i} \tanh\left(\frac{u_i}{u_{M_i}}\right) = u_{M_i} \frac{e^{\frac{u_i}{u_{M_i}}} - e^{-\frac{u_i}{u_{M_i}}}}{e^{\frac{u_i}{u_{M_i}}} + e^{-\frac{u_i}{u_{M_i}}}} \tag{11}$$

Then $sat(u_i(t))$ in (5) can be expressed as follows

$$sat\big(u_i(t)\big) = g(u_i) + d(u_i) = u_{M_i} \tanh\left(\frac{u_i}{u_{M_i}}\right) + d(u_i) \tag{12}$$

Where $d(u_i) = sat(u_i) - g(u_i)$ is a bounded function, and its bound can be obtained as

$$|d(u_i)| = |sat(u_i) - g(u_i)| \le u_{M_i}(1 - \tanh(1)) = 0.2785 u_{M_i} \tag{13}$$

So, the system can be written as

$$\dot{\eta} = q(\eta, \psi) \tag{14}$$

$$\dot{\psi}_k^j = \psi_{k+1}^j, \quad 1 \le k \le r_j - 1, \ 1 \le j \le m$$

$$\dot{\psi}_{r_j}^j = b_j(\eta, \psi) + \textstyle\sum_{i=1}^{m} a_{ji}(\eta, \psi)\, g(u_i) + M_j(t) \tag{15}$$

Where $M_j(t) = \sum_{i=1}^{m} a_{ji}(\eta, \psi)\, d(u_i) + \Delta d_j(t)$, $|M_j| \le D_j$, $D_j = \left|0.2785 a_{j,imax} u_{M_j}\right| + \Delta d_{jmax}$

In the paper, assumptions are made regarding the system (8) consistently.

Assumption 1. The nonlinear plant (8) is feedback linearizable without saturation [15].

Assumption 2. The desired trajectory y_{d_i} and its r_j − th derivatives are known, bounded, and piecewise continuous.

Assumption3. Zero dynamic system $\dot{\eta} = q(\eta, \psi)$ is input-to-state stable.

Definition 1. A function N(s) is considered a Nussbaum-type function when it possesses the properties listed [28, 18, 29].

$$\lim_{s \to \pm\infty} \sup \frac{1}{s} \int_0^s N(\mathcal{X}) d\mathcal{X} = \infty, \tag{16}$$

$$\lim_{s \to \pm\infty} \inf \frac{1}{s} \int_0^s N(\mathcal{X}) d\mathcal{X} = -\infty, \tag{17}$$

According to the definition, Nussbaum functions must possess infinite gains and infinite switching frequencies. Multiple functions that meet these criteria are $\mathcal{X}^2 \cos(\mathcal{X})$, $\mathcal{X}^2 \sin(\mathcal{X})$, $e^{\mathcal{X}^2} \cos(\frac{\pi}{2}\mathcal{X})$, and $e^{\mathcal{X}^2} \sin(\frac{\pi}{2}\mathcal{X})$. The paper utilizes the Nussbaum function $\mathcal{X}^2 \cos(\mathcal{X})$. The following lemma presents the property of Nussbaum functions, as stated in reference [29].

Lemma 1 [29]*:* Smooth functions $V(.)$ and $\mathcal{X}(.)$ are defined on $[0, t_f)$ with $V(t) \ge 0, \forall t \in [0, t_f)$, and $\mathcal{N}(\mathcal{X})$is a Nussbaum gain function. If the inequality is satisfied, $V(.)$ and $\mathcal{X}(.)$ must be limited on the interval $[0, t_f)$.

$$V \le V(0) e^{-Ct} + \frac{M}{C}(1 - e^{-Ct}) + \frac{e^{-Ct}}{\gamma_{\mathcal{X}}} \int_0^t (\xi \mathcal{N}(\mathcal{X}) \dot{\mathcal{X}} - \dot{\mathcal{X}}) e^{C\tau} \, d\tau \tag{18}$$

where $C > 0, M > 0, \gamma_{\mathcal{X}} > 0$ are constants, and ξ is a positive variable.

3.3 . Design of integral backstepping sliding mode controller and stability analysis

This section combines the backstepping method and sliding mode control to create a backstepping-sliding-mode controller that achieves robust control for uncertain systems. The backstepping technique designs a virtual control law that can guarantee the tracking error converges to zero asymptotically. The SMC technique is then used to create a robust control law that can compensate for the uncertainties and disturbances in the system. Backstepping control is combined with integral action to reduce the steady-state bias or decrease the rising time. Considering the system in (10), the integral backstepping can be implemented by incorporating the integral term of the tracking error $\int_0^t \left(\psi_j(\tau) - \psi_{d_j}(\tau)\right) d\tau$ at the initial stage of backstepping. The system remains in strict feedback form, but the relative degree of each output vector is increased to $r_j + 1$, requiring $r_j + 1$ steps of backstepping. In addition, to tackle the challenge of input saturation, the control scheme incorporates a novel auxiliary design system and Nussbaum gain functions. The auxiliary design system enables the design of a control law that effectively manages input saturation. At the same time, the Nussbaum gain functions contribute to the robustness of the control scheme, ensuring accurate tracking of the target trajectory despite input saturation.

$$\dot{\psi}_{j,1} = \psi_{j,2} - \psi_{d_j}$$

$$\dot{\psi}_{j,2} = \psi_{j,3}$$

$$\vdots$$

$$\dot{\psi}_{j,r_j+1} = b_j(\eta, \psi) + \sum_{i=1}^{m} a_{ji}(\eta, \psi)\, g(u_i) + M_j(t)$$

$$i = j = 1, 2, \cdots, m$$

$$\dot{\eta} = q(\eta, \psi)$$

$$y_j = \psi_{j,2} \tag{19}$$

$$\dot{u}_i = -k_i u_i + w_i \quad (20)$$

Where k_i are positive constants and w_i are auxiliary signals to be designed in the backstepping approach. Consequently, the control law design switches to design w_i. It is evident that all functions in equations (19) and (20) are continuous, and backstepping can be successfully applied. The design has a procedure of r_j+1 steps for each subsystem, which has a relative degree of order r_j. An error variable z_i is defined at each step, and a stabilizing function α_i is created to stabilize an ith-order subsystem concerning a Lyapunov function V_i. The state feedback control is provided in the final stage. The structure of the closed-loop system is depicted in Fig. 2.

Remark 1: System (19) contains the function $g(u_i)$, which acts as a 'control input' for systems studied with backstepping techniques. Designing the control signal u_i without using a direct method is challenging in our current scenario. To address this issue, we intentionally include (20) to generate a reliable control signal u_i by establishing an auxiliary control signal w_i during the last step $r_j + 2$ of the backstepping procedure [18].

***Remark 2*:** The augmented systems (19) and (20) vary from the ones examined with the conventional backstepping method. This occurs because $\dot{\psi}_{r+1}$ has a direct relationship with the non-linear function $g(u_i)$ rather than u_j. This leads to a term of $(\frac{\partial g}{\partial u_i})\dot{u}_i$ instead of $\dot{u}_i$, which differs from prior backstepping strategies. To handle this issue, a Nussbaum function is utilized.

In the usual backstepping method for tracking issues, a coordinate transformation is carried out for $j-th$ output.

$$z_{j,1} = \psi_{j,1} = \int_0^t (\psi_{j,2} - \psi_{d_j}) d\tau \quad (21)$$

$$z_{j,i} = \psi_{j,i} - \psi_{d_j}^{(i-2)} - \alpha_{j,i-1},\ i = 2, \cdots, r+1, \quad (22)$$

$$z_{j,r+2} = g(u) - \alpha_{j,r+1} \quad (23)$$

Where $\alpha_{j,i-1}$ represents the virtual control input that needs to be determined at the ith step, the introduction of variable $z_{j,r+2}$ arises from including the new state variable u. In the subsequent sections, an integral backstepping sliding mode control scheme will be proposed for controlling an $n-th$ order system with relative degree $r < n$, satisfying assumptions 1-3. For clarity and brevity, only the first and the last two steps of the design procedure will be elaborated in detail, focusing on the methodology employed to handle $g(u)$.

Step i $(i = 1,2, \cdots, r)$: We choose the virtual control law $\alpha_{j,i}$ as

$$\alpha_{j,1}(z_{j,1}) = -c_{j,1} z_{j,1} \quad (24)$$

$$\alpha_{j,i} = -c_{j,i} z_{j,i} - z_{j,i-1} + \sum_{i=1}^{i-1} \left(\frac{\partial \alpha_{j,i-1}}{\partial \psi_{j,i}} \psi_{j,i+1} + \frac{\partial \alpha_{j,i-1}}{\partial \psi_{dj}^{(i-1)}} \psi_{dj}\right) \quad (25)$$

Where $c_{j,i}$ are positive design parameters. The Lyapunov function is suggested as

$$V_{j,i} = \sum_{i=1}^{i} \frac{1}{2} z_{j,i}^2 \quad (26)$$

Then, the derivative of $V_{j,i}$, along with (21) and (22), is given by

$$\dot{V}_{j,i}(z_{j,1}, z_{j,2}, \cdots, z_{j,i}) = -\sum_{i=1}^{i} c_{j,i} z_{j,i}^2 + z_{j,i} z_{j,i+1} \quad (27)$$

Step $k = r + 1$: The time derivative of the tracking error z_k from (19) and (22) is derived as given below

$$\dot{z}_{j,k} = \dot{\psi}_{j,k} - \psi_{d_j}^{(k-1)} - \dot{\alpha}_{j,k-1} = b_j(\eta, \psi) + a_j(\eta, \psi)(z_{jk+1} + \alpha_{jk}) + M_j(t) - \psi_{d_j}^{(k-1)} - \dot{\alpha}_{j,k-1} \quad (28)$$

where $g(u) = z_{j,k+1} + \alpha_{j,k}$ has been used. we design the virtual control law α_k as follows

$$\alpha_{j,k} = a_j(\eta, \psi)^{-1}[-c_{j,k} z_{j,k} - z_{j,k-1} - b_j(\eta, \psi) + \psi_{d_j}^{(k-1)} - M_j(t) + \dot{\alpha}_{j,k-1}] \quad (29)$$

Incorporating a switch item into $\alpha_{j,k}$ with $s_j = z_{j,k}$ as the sliding surface helps maintain robust performance despite uncertainties and external disturbances $M_j(t)$. Therefore, the virtual control α_{jk} is structured in this manner.

$$\alpha_{jk} = a_j(\eta, \psi)^{-1}[-c_{j,k} z_{j,k} - z_{j,k-1} - b_j(\eta, \psi) + \psi_{d_j}^{(k-1)} - D_j sgn(z_{j,k}) + \dot{\alpha}_{j,k-1}] \quad (30)$$

The discontinuity of the $sign(.)$ function introduces non-differentiability issues, hindering the subsequent design procedure. The hyperbolic tangent function can replace the discontinuous $sign(.)$ function in (30) to overcome this challenge and obtain a smooth control signal. Ultimately, the stabilizing function α_k is verified as the following

$$\alpha_{j,k} = a_j(\eta, \psi)^{-1}[-c_{j,k} z_{j,k} - z_{j,k-1} - b_j(\eta, \psi) + \psi_{d_j}^{(k-1)} - D_j tanh\left(\frac{z_{j,k}}{\varepsilon_j}\right) + \dot{\alpha}_{j,k-1}] \quad (31)$$

$\varepsilon > 0$ is the boundary layer coefficient. Define a new Lyapunov function candidate

$$V_{j,k}(z_{j,1}, z_{j,2}, \cdots, z_{j,k}) = V_{j,k-1} + \frac{1}{2} z_{j,k}^2 \quad (32)$$

that its time-derivative, along with (27) and (28), is given by

$$\begin{aligned}\dot{V}_{j,k} &= \dot{V}_{j,k-1} + z_{j,k}\dot{z}_{j,k} = -\sum_{i=1}^{k-1} c_{j,i} z_{j,i}^2 + z_{j,k-1} z_{j,k} \\ &+ z_{j,k}[b_j(\eta, \psi) + a_j(\eta, \psi) z_{j,k+1} - c_{j,k} z_{j,k} - z_{j,k-1} \\ &- b_j(\eta, \psi) + \psi_{d_j}^{(k-1)} - D_j tanh\left(\frac{z_{j,k}}{\varepsilon_j}\right) \\ &+ \dot{\alpha}_{j,k-1} + M_j(t) - \psi_{d_j}^{(k-1)} - \dot{\alpha}_{j,k-1}] \\ &= -\sum_{i=1}^{k} c_{j,i} z_{j,i}^2 - D_j z_{j,k} tanh\left(\frac{z_{j,k}}{\varepsilon_j}\right) \\ &+ z_{j,k} M_j(t) + a_j(\eta, \psi) z_{j,k+1} z_{j,k}\end{aligned} \quad (33)$$

It is important to note that the following inequality remains valid for all values of $\varepsilon > 0$ [3, 29].

$$0 \le |z_{j,k}| - z_{j,k} \tanh\left(\frac{z_{j,k}}{\varepsilon_j}\right) \le c\varepsilon_j, \quad c = 0.2785 \quad (34)$$

After some arrangement, the following inequality can be obtained

$$\begin{aligned}&z_{jk} M_j - D_j z_{j,k} \tanh\left(\frac{z_{j,k}}{\varepsilon_j}\right) \le |z_{j,k}| M_j - \\ &D_j z_{kj,} \tanh\left(\frac{z_{j,k}}{\varepsilon_j}\right) \le |z_{j,k}| D_j - D_j z_{j,k} \tanh\left(\frac{z_{j,k}}{\varepsilon_j}\right) \le D_j c\varepsilon_j\end{aligned} \quad (35)$$

Associating with (33), (35) is formulated as

$$\dot{V}_{j,k} \le -\sum_{i=1}^{k} c_{j,i} z_{j,i}^2 + D_j c\varepsilon_j + a_j(\eta, \psi) z_{j,k+1} z_{j,k} \quad (36)$$

Step $k + 1$: From (19), (20), and (23), we obtain

$$\dot{z}_{j,k+1} = \frac{\partial g}{\partial u}(-ku + w)$$

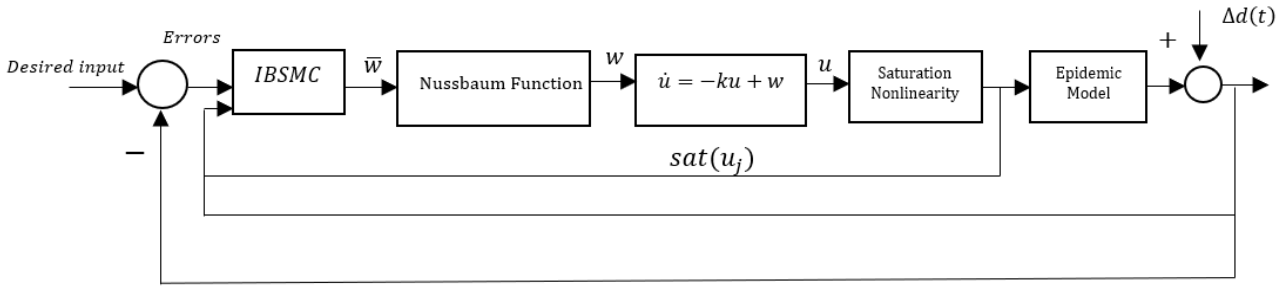

Fig.2. Schematic diagram of Integral backstepping sliding mode control strategy.

$$-\frac{\partial \alpha_{j,k}}{\partial \psi_{j,k}}\Big(b_j(\eta,\psi)+a_j(\eta,\psi)g(u)+M_j(t)\Big)-\Upsilon_j \quad (37)$$

$$\Upsilon_j=\sum_{i=1}^{k-1}\frac{\partial \alpha_{j,k}}{\partial \psi_{j,i}}\psi_{j,i+1}+\sum_{i=1}^{k}\frac{\partial \alpha_{j,k}}{\partial \psi_{d_j}^{(k-1)}}\psi_{d_j}^{(k)} \quad (38)$$

Remember that $\frac{\partial g}{\partial u}$ is a quantity that changes, adding complexity to the design and analysis procedures. To address this challenge, we introduce the Nussbaum function $N(\chi)$ as follows

$$\mathcal{N}(\mathcal{X})=\mathcal{X}^2\cos(\mathcal{X}) \quad (39)$$

A design for the backstepping control law for w is formulated in the following manner:

$$w=\mathcal{N}(\mathcal{X})\bar{w} \quad (40)$$

$$\dot{\mathcal{X}}=\gamma_{\mathcal{X}}z_{k+1}\bar{w} \quad (41)$$

$$\bar{w}=-c_{j,k+1}z_{j,k+1}+\frac{\partial \alpha_{j,k}}{\partial \psi_{j,k}}\Big(b_j(\eta,\psi)+a_j(\eta,\psi)g(u)\Big)+\Upsilon_i+\frac{\partial g}{\partial u}ku-a_j(\eta,\psi)z_{j,k}-\mathcal{L}_j\left(\frac{\partial \alpha_{j,k}}{\partial \psi_{j,k}}\right)^2 z_{j,k+1} \quad (42)$$

The coefficients $c_{k+1}, \mathcal{L}$, and $\gamma_{\mathcal{X}}$ are positive accurate design parameters. To analyze the designed system, we now consider an augmented positive Lyapunov function given by:

$$V_{j,k+1}\big(z_{j,1},z_{j,2},\cdots,z_{j,n+1}\big)=V_{j,k}+\frac{1}{2}z_{j,k+1}^2 \quad (43)$$

The derivative of $V_{j,k+1}$ is given

$$\begin{aligned}\dot{V}_{j,k+1}&=-\sum_{i=1}^{k}c_{j,i}z_{j,i}^2+a_j(\eta,\psi)z_{j,k}z_{j,k+1}+D_jc\varepsilon_j\\&\quad+z_{j,k+1}\big(\dot{z}_{j,k+1}+\bar{w}-\bar{w}\big)\\&=-\sum_{i=1}^{k}c_{j,i}z_{j,i}^2-a_j(\eta,\psi)z_{j,k}z_{j,k+1}+D_jc\varepsilon_j\\&\quad-z_{j,k+1}\bar{w}\\&\quad+z_{j,k+1}\left(\frac{\partial g}{\partial u}w-c_{j,k+1}z_{j,k+1}-a_j(\eta,\psi)z_{j,k}-\frac{\partial \alpha_k}{\partial \psi_k}M_j-\mathcal{L}_j\left(\frac{\partial \alpha_{j,k}}{\partial \psi_{j,k}}\right)^2 z_{j,k+1}\right)\\&\le-\sum_{i=1}^{k+1}c_{j,i}z_{j,i}^2+D_jc\varepsilon_j-z_{j,k+1}\bar{w}+z_{j,k+1}\frac{\partial g}{\partial u}w\\&\quad-z_{j,k+1}\frac{\partial \alpha_{j,k}}{\partial \psi_{j,k}}M_j-\mathcal{L}_j\left(\frac{\partial \alpha_{j,k}}{\partial \psi_{j,k}}\right)^2 z_{j,k+1}^2\end{aligned} \quad (44)$$

Substituting (40) and (41) into (44) and utilizing $ab\le\frac{a^2}{2}+\frac{b^2}{2}$, we obtain

$$\dot{V}_{j,k+1}\le-C_jV_{j,k+1}+D_jc\varepsilon_j+\frac{1}{\gamma_{\mathcal{X}_j}}(\xi\mathcal{N}(\chi)-1)\dot{\chi}+\frac{1}{4\mathcal{L}_j}D_j^2 \quad (45)$$

Where $C_j=2min\{c_{j,1},c_{j,2},\cdots,c_{j,k+1}\}$. Define $\frac{\partial g}{\partial u}=\xi$ and $\left|\frac{\partial g}{\partial u}\right|=\left|\frac{4}{(e^{\frac{v}{u_M}}+e^{-\frac{v}{u_M}})^2}\right|\le 1$.

By directly integrating differential inequality (45), we obtain

$$V_{j,k+1}\le V_{j,k+1}(0)e^{-C_jt}+\frac{1}{C_j}\left(D_jc\varepsilon_j+\frac{D_j^2}{4\mathcal{L}_j}\right)\big(1-e^{-C_jt}\big)+\frac{e^{-C_jt}}{\gamma_{\mathcal{X}_j}}\int_0^t(\xi\mathcal{N}(\chi)-1)\dot{\chi}e^{C_j\tau}d\tau \quad (46)$$

We can conclude that the closed-loop system is stable based on Lemma 1.

Theorem 1. Consider the uncertain nonlinear system (8) satisfying Assumptions 1–3 and Lemma 1. An integral backstepping sliding mode control (42) makes outputs $y_j(t)$ track the desired trajectory $y_{d_j}(t)$ while ensuring the boundedness of all the closed-loop signals.

Proof. By applying the virtual controllers (24), (25), and (29), along with the Lyapunov functions (26), (32), and (43), and control law (40), the stability of the closed-loop system is ensured.

4. Result and Discussion

In this section, we apply the proposed controller scheme to an uncertain SEIAR influenza epidemiological model with three saturated control inputs. The system dynamics take into account input saturation, uncertainty, and external disturbances. The values of the influenza epidemic parameters used in the simulations are obtained from [10, 30] are provided in Table I. We validate the effectiveness of the proposed system through simulation analysis conducted in the MATLAB Simulink environment. The performance of the proposed controller is compared with two other controllers: the dynamic anti-windup compensator (AWC) and the adaptive sliding mode controller (ASMC), as described in [13] and [31]. In [31] an anti-windup compensator is implemented to address the effects of actuator saturation using a two-step design technique. First, a nonlinear dynamic feedback controller is designed based on feedback linearization without considering input constraints. Then, a dynamic

compensator is added to account for saturation. In this technique, the difference between the control signal generated by the controller and the actuator's saturated signal serves as the dead-zone signal, which activates the anti-windup compensator.
We assume the following saturation levels for the control inputs:

$$\mathrm{sat}(u_1) = \begin{cases} 0.8, & u_1 \geq 0.8 \\ u_1, & 0 \leq u_1 \leq 0.8 \\ 0, & u_1 \leq 0 \end{cases}$$
$$sat(u_2) = \begin{cases} 0.5, & u_2 \geq 0.5 \\ u_2, & 0 \leq u_2 \leq 0.5 \\ 0, & u_2 \leq 0 \end{cases} \quad (47)$$
$$sat(u_3) = \begin{cases} 0.3, & u_3 \geq 0.3 \\ u_3, & 0 \leq u_3 \leq 0.3 \\ 0, & u_3 \leq 0 \end{cases}$$

The simulations are based on a final treatment time of $t_f = 50$ days, representing the duration for eradicating the disease in the population, as determined by the designer. The running time of algorithm implementation is 2.58 seconds. To control the influenza epidemic, the target reduction of the susceptible and infected compartments (I_d, E_d, S_d) over time is defined as follows:

$$I_d = (I_0 - I_f)\exp(-at) + I_f$$
$$E_d = (E_0 - E_f)\exp(-at) + E_f \quad (48)$$
$$S_d = (S_0 - S_f)\exp(-at) + S_f$$

Where $\boldsymbol{a}$ is the adjustable population reduction rate and is chosen as $\boldsymbol{a} = 0.2$. I_f, E_f, and S_f are the desired steady-state numbers of infected, exposed, and susceptible individuals, respectively, they are assumed to be zero ($I_f = 0,\ E_f = 0,\ S_f = 0$). I_0, E_0, and S_0 are the initial numbers of infected, exposed, and susceptible persons. The initial values of the influenza variables in these simulations are also given in Table II. Parameters in controller laws are presented in Table III. Additionally, a maximum of 80% uncertainty is taken into account for the initial estimation of model parameters ($\hat{\theta} = 1.8\theta$), while $\Delta d(t) =$
$[\,0.3\sin(4t)\ \ 0.5\sin(3t)\ \ 0.8\cos(2t)\ 0.2\sin(5t)\ 0.4\cos(t)]^T$
represents unidentified time-varying external disturbances, unmodeled dynamics, and perturbations introduced into the system.

Table I. Parameters of the epidemiological model [30]

Parameter	Description	Values
κ	Rate of becoming infectious after a latent period	$0.833\mathrm{days}^{-1}$
γ	The cure rate for the infected	$0.833\mathrm{days}^{-1}$
η	The cure rate for the Asymptomatic	$0.244\mathrm{days}^{-1}$
p	Percentage of experiencing symptoms.	$0.667\mathrm{days}^{-1}$
β	Transmission rate	$1.66\ \mathrm{days}^{-1}$
μ	Natural death rate	$0.00392\mathrm{days}^{-1}$
υ	Rate of birth	$0.0086\mathrm{days}^{-1}$
ρ	disease caused death rate	$0.02\mathrm{days}^{-1}$
ω	Rate of losing immunity	$0.833\ \mathrm{days}^{-1}$

Table II. Initial values of the state and the controller variables

Variable	Initial value
S_0	400
E_0	150
I_0	250
A_0	100
R_0	100
$u_1(0)$	10
$\boldsymbol{u_2(0)}$	10
$\boldsymbol{u_3(0)}$	0
$\chi_1(0)$	1
$\chi_2(0)$	3
$\chi_3(0)$	2

Table III. Control Parameters

Parameter	Description	Values
k	$[k_1\ k_2\ k_3]$	[20 10 10]
γ_x	$[\gamma_{x_1}\ \gamma_{x_2}\ \gamma_{x_3}]$	[0.01 0.01 0.01]
$\mathcal{L}$	$[\mathcal{L}_1\ \mathcal{L}_2\ \mathcal{L}_3]$	[5 10 5]
ε	$[\varepsilon_1\ \varepsilon_2\ \varepsilon_3]$	[1 1 0.8]
c	$[c_{11}\ c_{12}\ \cdots\ c_{33}]$	[5 5 5 5 5 5 10 100 100]

The text presents a comparative analysis of three simulation scenarios to investigate the population dynamics of the SEIAR mathematical model under varying conditions. These scenarios encompass:

(I) Absence of control measures: This scenario serves as a baseline to observe the model's behavior without any interventions.

(II) Application of different controllers on an unconstrained System: Here, various controllers are applied to the model without considering any constraints. This allows for an assessment of the controllers' effectiveness in an ideal setting.

(III) Examination of the input-constrained System: in this scenario, the model incorporates input constraints, reflecting real-world limitations. The performance of the

proposed dynamic compensator, AWC, and adaptive SMC is evaluated under these constraints.

The comparison of these scenarios provides insights into the impact of control strategies and saturation constraints on the population dynamics of the SEIAR model. It highlights the need for careful controller design and consideration of practical limitations to achieve adequate disease control.

Fig. 3 illustrates the temporal evolution of the respective populations in the absence of control measures. Using the parameters from Table 2, the basic reproduction number is calculated to be ($R_0 = 4.0463$) which is greater than 1. Consequently, the disease becomes uniformly persistent and converges to its endemic equilibrium point of (658, 137, 123, 146, 126). As a result, the population will always have several infectious and asymptomatic individuals. This implies that natural disease eradication is impossible. To control the pandemic diseases, disease time control has more priority and we should be able to drive the disease model to the disease-free equilibrium point in the shortest possible time. Consequently, a control action must be applied to eradicate the disease. In Fig. 4. an unconstrained system is controlled using integral backstepping sliding mode control, anti-windup compensator, and adaptive sliding mode control. Upon incorporating the proposed control measures, including vaccination, antiviral treatment, and social distancing, it is observed that the basic reproduction number decreases rapidly as the disease outbreak progresses. Eventually, the model returns to a disease-free state (0,0,0,0, N) as time approaches infinity. As a result, the numbers of susceptible (S), exposed (E), and infected (I) individuals decrease to zero, achieving the desired tracking goal for these influenza compartments. Additionally, the population of asymptomatic individuals (A) declines towards zero due to the decreasing numbers in the S, E, and I, compartments. Furthermore, the number of recovered individuals (R) increases and asymptotically approaches the total population. As illustrated in the figure, the AWC controller is unable to handle uncertainties and external disturbances, resulting in a negative susceptible population, which is unrealistic. In contrast, the proposed controller exhibits superior convergence speed and tracking accuracy in controlling the unconstrained epidemic disease compared to the other two controllers.

Now, consider a scenario where the control inputs are limited. When the actuator becomes saturated, feedback loops are disrupted, preventing the controller from effectively influencing system performance. Consequently, saturation issues can lead to significant performance degradation, resulting in oscillations, prolonged settling times, undershoots, delays, excessive overshoots, and instability. Figure 5 illustrates the output of the constrained system under various control strategies after 50 days of treatment. As depicted, the degradation of the uncompensated system is evident in the output responses, which exhibit undesirable oscillations and prolonged settling times, ultimately compromising control performance. As a result, during the treatment period, a portion of the population remains susceptible, and recovered individuals are unable to fully converge to the total population. After applying various control strategies to the constrained system, it is clear that overall system performance has improved. The IBSMC approach presents several advantages compared to other methods. It achieves superior tracking accuracy by minimizing discrepancies between actual system states and desired trajectories. Additionally, it effectively addresses input saturation, ensuring that control inputs stay within feasible limits while preserving stability and performance. The approach enhances stability by incorporating integral action, which eliminates steady-state errors and improves overall robustness, even in the presence of uncertainties and disturbances. As illustrated in Figure 5(a), on day 50, the difference in the number of susceptible individuals between the cases with and without the anti-windup compensator is approximately 360 individuals. This demonstrates that even when the vaccination input is saturated, the proposed controller effectively mitigates the negative impacts of input constraints, leading to a reduction in the number of susceptible individuals. Furthermore, as shown in Figure 5(b), when saturation occurs with the proposed compensator, the number of recovered individuals increases over time and converges toward the final population (N). This behavior demonstrates the controller's ability to maintain stability and ensure that the system reaches the desired equilibrium point, even in the presence of input saturation.

Based on the information presented in Figures 5(c) and 5(d), the convergence rate to zero for infected and exposed individuals is significantly faster when the proposed IBSMC compensator is employed compared to other methods. This is a crucial factor in managing pandemic diseases, as it is essential to control the timing of the disease to quickly steer the model toward a disease-free equilibrium point. The faster convergence rate achieved by the IBSMC compensator is attributed to its improved tracking accuracy, robustness to input saturation, enhanced stability, and adaptability. These advantages allow the IBSMC controller to respond effectively to changes in the epidemic dynamics and to drive the system towards the desired disease-free equilibrium point more rapidly. The implementation of the proposed compensator reduces the eradication duration of infected and exposed individuals by approximately 15 days compared to scenarios without it. By reducing the eradication duration of infected and exposed individuals, the IBSMC compensator can potentially mitigate the impact of the pandemic, reduce the burden on healthcare systems, and save lives.

The implemented rates of vaccination (u_1) for the susceptible individuals, social distancing measures (u_2) for the exposed individuals, and antiviral treatment rates (u_3) for the infected individuals before and after saturation are illustrated in Fig 6. It is important to note that the vaccination, social distancing, and antiviral treatment rates in this model must be less than 1 ($0 \le u_1(t) \le 1, 0 \le u_2(t) \le 1,$ and $0 \le u_3(t) \le 1$). This constraint ensures that the control inputs remain within feasible ranges. The simulation results demonstrate that the obtained control inputs satisfy this implementation constraint. This ensures that the control

strategies are practically implementable and do not violate any physical or biological constraints.

The tracking errors for the susceptible, exposed, and infected compartments of the input-saturated system relative to their desired values are presented in Fig. 7, comparing the proposed IBSMC control, dynamic anti-windup control, and adaptive sliding mode control. The IBSMC control scheme allows the system to accurately follow a desired trajectory while minimizing the tracking errors between the actual system states and the intended trajectory. This control approach enhances the system's stability and performance by keeping tracking errors small, thereby achieving more precise control over the compartments within the system.

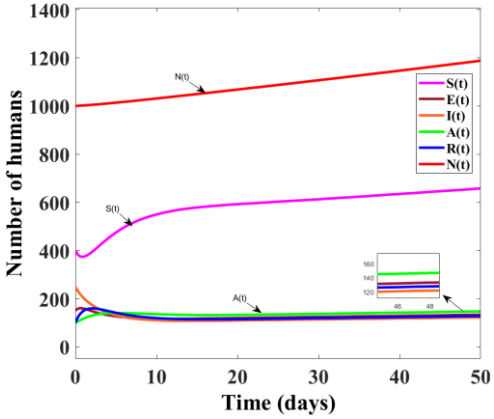

Fig. 3. Time evolution of individual populations over time in the absence of control measures.

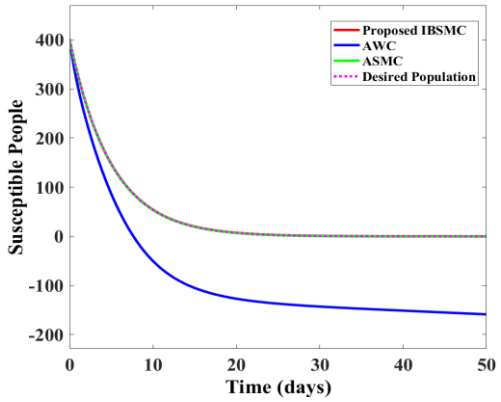

(a)

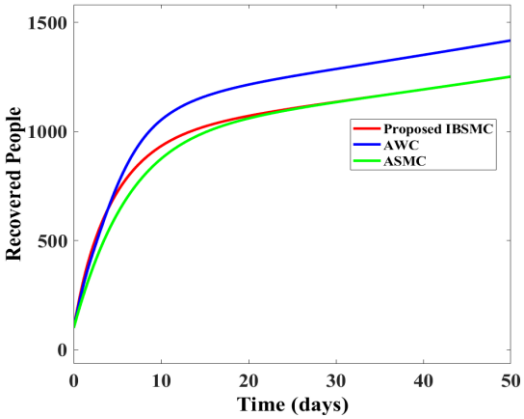

(b)

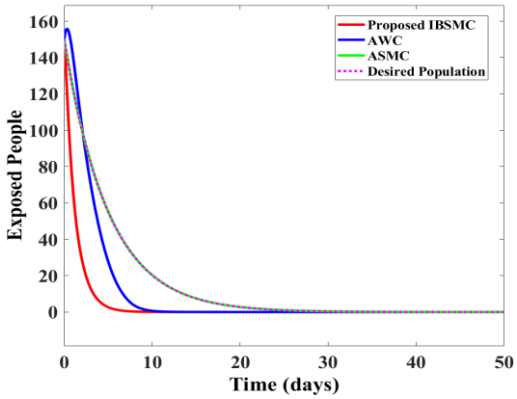

(c)

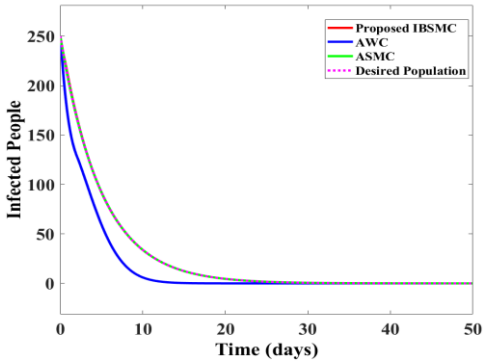

(d)

Fig. 4. State variables of the unconstrained system under different control strategies: (a) Susceptible, (b)Recovered, (c) Exposed, and (d) Infected population.

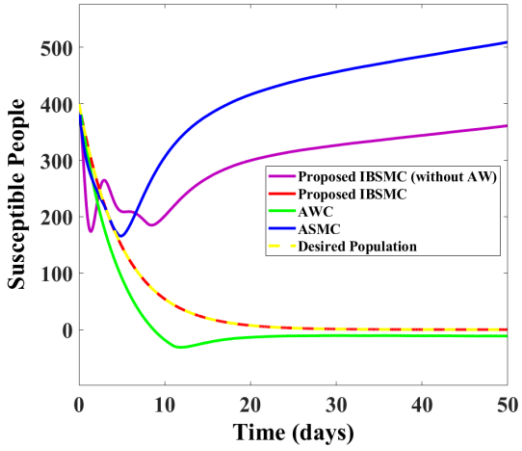

(a)

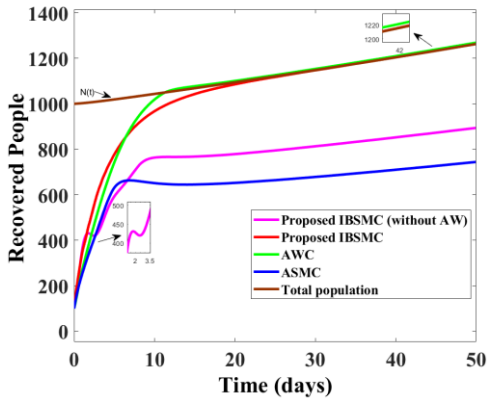

(b)

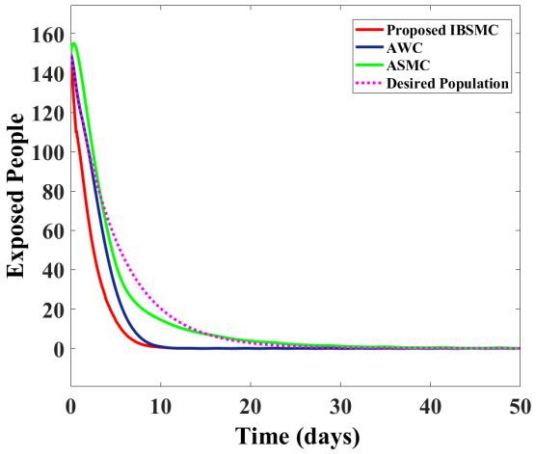

(c)

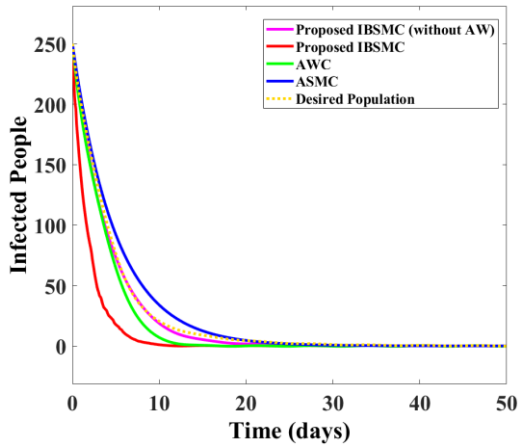

(d)

Fig. 5. State variables of the input-constrained system under different control strategies: (a) Susceptible, (b) Recovered, (c) Exposed, and (d) Infected Population

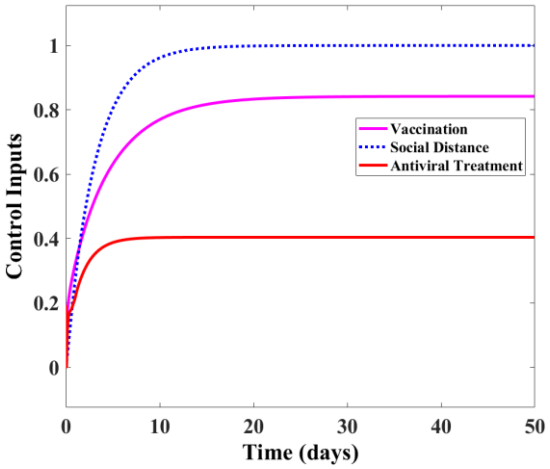

(a)

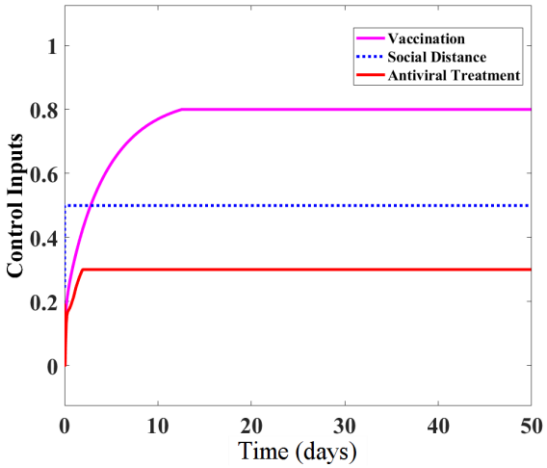

(b)

Fig. 6. Control inputs applied to SEIAR Epidemic model (a) befor saturation, and (b) after saturation.

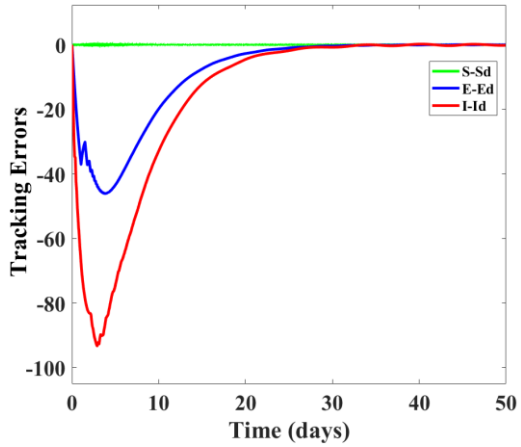

(a)

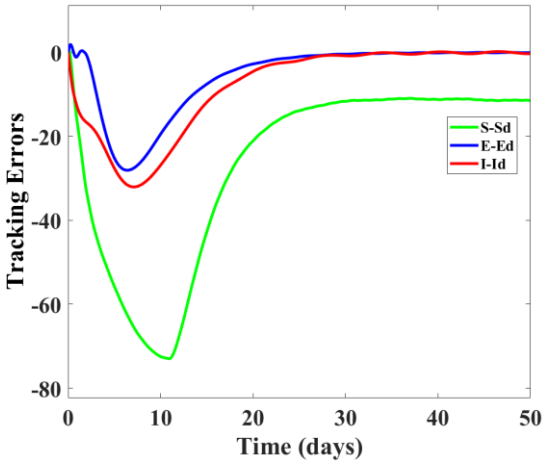

(b)

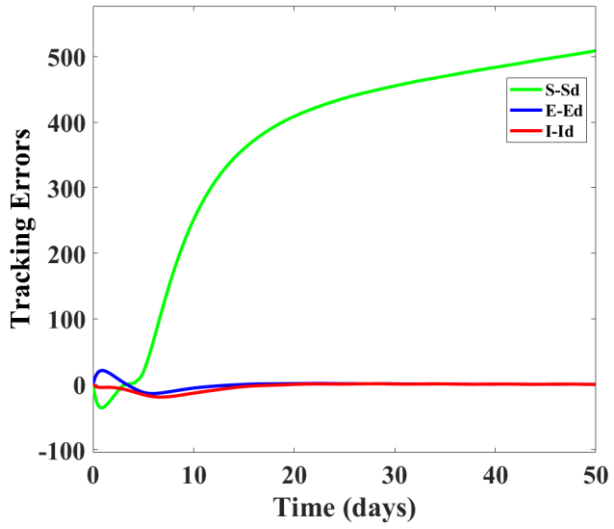

(c)

Fig. 7. Tracking errors of the susceptible, exposed, and infected populations relative to their desired values, using: (a) the proposed dynamic anti-windup, (b) the anti-windup compensator presented, and (c) adaptive sliding mode control.

5. Conclusion

This study investigates the efficiency of an anti-windup compensation method on the MIMO epidemic system in the presence of input saturation. This is the first study to explore this specific epidemic modelling and control aspect. By considering input saturation and employing an anti-windup compensation method, the study aims to address practical constraints and improve the robustness and performance of the epidemic control system. The nonlinear integral backstepping sliding mode control strategy, which combines the advantages of sliding mode control and backstepping control, is proposed to address the spread of epidemic diseases in a host population. A SEIAR epidemic model with uncertain parameters is employed to describe the spread of the disease, taking into account the dynamic population. Taking into account the uncertainties in the nonlinear dynamics of the model, the controller can better handle variations and unexpected changes in the disease transmission process, leading to improved control performance and resilience in the face of real-world challenges. The proposed control strategy with three control inputs aims to reduce the susceptible, infected, exposed, and asymptomatic individuals to zero while maximizing the recovered population by tracking the total population. Simulation results demonstrate that the proposed IBSMC control scheme effectively addresses the challenges posed by input saturation and external disturbances, ensuring the stability of the nonlinear uncertain MIMO epidemic system and achieving the desired trajectory tracking performance. In practical situations, the quantity of people in each group may not be easily accessible, so developing a control method using observer output for the epidemic model is crucial. Future studies will investigate design methods based on observers and effective control strategies for nonlinear epidemic and biological systems.

6. References

[1] A. H. Amiri Mehra, I. Zamani, Z. Abbasi and A. Ibeas, "Observer-based adaptive PI sliding mode control of developed uncertain SEIAR influenza epidemic model considering dynamic population," *Journal of Theoretical Biology,* vol. 482, p. 109984, 2019.

[2] Z. Abbasi, I. Zamani, A. H. Amiri Mehra, M. Shafieirad and A. Ibeas, "Optimal Control Design of Impulsive SQEIAR Epidemic Models with Application to COVID-19," *Chaos, Solitons & Fractals,* vol. 139, p. 110054, 2020.

[3] A. Rajaei, M. Raeiszadeh, V. Azimi and M. Sharifi, "State estimation-based control of COVID-19 epidemic before and after vaccine development," *Journal of Process Control,* vol. 102, pp. 1-14, 2021.

[4] I. Sekkak, B. R. Nasri, B. N. Rémillard, J. Dzevela Kong and M. El Fatini , "A stochastic analysis of a SIQR epidemic model with short and long-term prophylaxis," *Communications in Nonlinear Science and Numerical Simulation,* vol. 127, p. 107523, 2023.

[5] A. I. Abioye, J. P. Olumuyiwa, A. O. Hammed, A. O. Festus, O. Kayode, A. I. Abdullahi and K. Ilyas, "Mathematical model of COVID-19 in Nigeria with optimal control," *Results in Physics,* vol. 28, p. 104598, 2021.

[6] S. Muthukumar, A. Balakumar, S. Ravikumar and V. Chinnadurai, "An optimal control of bi-modal COVID-19 SEIQR epidemic spreading model in India," *Results in Control and Optimization,* vol. 12, p. 100256, 2023.

[7] F. Khondaker, "Optimal control analysis of Influenza epidemic model," *Applied Mathematics,* vol. 13, pp. 845-857, 2022.

[8] S. Adak and S. Jana, "Dynamical behavior of an epidemic model with fuzzy transmission and fuzzy treatment control," *Journal of Applied Mathematics and Computing,* vol. 68, p. 1929–1948, 2022.

[9] H. Musadaq and Z. M. Amean, "New strategy to control covid-19 pandemic using lead/lag compensator," *Biomedical Signal Processing and Control,* vol. 68, p. 102669, 2021.

[10] M. De la Sen, A. Ibeas and S. Alonso-Quesada, "On vaccination controls for the SEIR epidemic model," *Communications in Nonlinear Science and Numerical Simulation,* vol. 17, no. 6, pp. 2637-2658, 2012.

[11] L. Zhou, J. Li, . D. Shi, L. Xu and S.-X. Huang, "Predicting Influenza Epidemic for United States," *International Journal of Environmental Health Research ,* vol. 32, no. 6, pp. 1231-1237, 2022.

[12] A. Veisi and H. Delavari, "Fractional-order backstepping strategy for fractional-order model of COVID-19 outbreak," *Mathematical Methods in the Applied Sciences,* vol. 45, no. 7, pp. 3479-3496, 2021.

[13] M. Sharifi and H. Moradi, "Nonlinear robust adaptive sliding mode control of influenza epidemic in the presence of uncertainty," *Journal of Process Control,* vol. 56, pp. 48-57, 2017.

[14] V. Azimi, M. Sharifi, S. Fakoorian, T. Nguyen and V. Huynh, "State estimation-based robust optimal control of influenza epidemics in an interactive human society," *Information Sciences,* vol. 592, pp. 340-360, 2022.

[15] J. Ibarra, R. Márquez and M. Bernal, "An LMI backstepping generalization via H-infinity dynamic control and Takagi-Sugeno models," *Fuzzy Sets and Systems,* vol. 495–496, p. 109085, 2024.

[16] T. Kuniya and H. Sano, "Application of the backstepping method to the prediction of increase or decrease of infected population," *Theoretical Biology and Medical Modelling,* vol. 13, pp. 1-10, 2016.

[17] M. L. Srief, B. Soltane, N. A. Lokmane and G. Malak, "A complete control structure based backstepping controller design for stacked multi-cell multi-level SPWM VSC STATCOM," *Energy Reports,* vol. 12, pp. 687-698, 2021.

[18] C. Wen, . J. Zhou, . Z. Liu and H. Su, "Robust Adaptive Control of Uncertain Nonlinear Systems in the Presence of Input Saturation and External Disturbance," *IEEE Transactions on Automatic Control,* vol. 56, pp. 1672-1678, 2011.

[19] Z. Fallah, M. Baradarannia, . H. Kharrati and F. Hashemzadeh, "Sliding Mode H∞ Control of Discrete-time Delayed Singular Markovian Jump Systems," *Tabriz Journal of Electrical Engineering,* vol. 54, no. 2, pp. 229-237, 2024.

[20] M. Wan, M. Chen and M. Lungu, "Integral Backstepping Sliding Mode Control for Unmanned Autonomous Helicopters Based on Neural Networks," *Drones ,* vol. 7, p. 154, 2023.

[21] A. K. Jain and S. Bhasin, "Robust backstepping control of uncertain nonlinear systems with unknown time-varying input delay," *IFAC-PapersOnLine,* vol. 53, no. 2, pp. 4862-4867, 2020.

[22] M. A. M. Basri, "Design and application of an adaptive backstepping sliding mode controller for a six-DOF quadrotor aerial robot," *Robotica,* vol. 36, no. 11, pp. 1701-1727, 2018.

[23] H. Shen, J. Iorio and N. Li, "Sliding Mode Control in Backstepping Framework for a Class of Nonlinear Systems," *journal of Marine Science and Engineering,* vol. 7, no. 12, p. 452, 2019.

[24] J. Keighobadi and M. m. Fateh, "Adaptive Robust Tracking Control Based on Backstepping Method for Uncertain Robotic Manipulators Including Motor Dynamics," *International Journal of Industrial Electronics Control and Optimization,* vol. 4, pp. 13-22, 2021.

[25] W. Guo and D. Liu, "Adaptive second-order backstepping control for a class of 2DoF underactuated systems with input saturation and uncertain disturbances," *Scientific Reports,* vol. 14, p. 15840, 2024.

[26] Y. Zhao, X. Sun, G. Wang and Y. Fan, "Adaptive Backstepping Sliding Mode Tracking Control for Underactuated Unmanned Surface Vehicle With Disturbances and Input Saturation," *IEEE Access,* vol. 9, pp. 1304-1312, 2020.

[27] S. Neisarian, M. M. Arefi, A. Abooee and S. Yin, "Fast finite-time observer-based sliding mode controller design for a class of uncertain nonlinear systems with input saturation," *Information Sciences,* vol. 630, pp. 599-622, 2023.

[28] M. Rostami, M. Shahriari-kahkeshi and H. Arvin, "Adaptive Improved Dynamic Surface Control for a Class of Uncertain Nonlinear Systems in the presence of Input Hysteresis and Unknown Control Direction," *Tabriz Journal of Electrical Engineering,* vol. 53, pp. 197-207, 2023.

[29] Y-J. Liu and . S. Tong, "Barrier Lyapunov functions for Nussbaum gain adaptive control of full state constrained nonlinear systems," *Automatica,* vol. 76, pp. 143-152, 2017.

[30] A. Ibeas, M. de la Sen and S. Alonso-Quesada, "Robust Sliding Control of SEIR Epidemic Models," *Mathematical Problems in Engineering,* vol. 2014, p. 104764, 2014.

[31] S.S. Yoon, J.K. Park and T.W. Yoon, "Dynamic anti-windup scheme for feedback linearizable nonlinear control systems with saturating inputs," *Automatica,* vol. 44, no. 12, pp. 3176-3180, 2008.